A developmental gene regulatory network for invasive differentiation of the *C. elegans* anchor cell

Taylor N. Medwig-Kinney[1,*], Jayson J. Smith[1,*], Nicholas J. Palmisano[1], Sujata Tank[1,2], Wan Zhang[1] and David Q. Matus[1,‡]

[1]Department of Biochemistry and Cell Biology, Stony Brook University, Stony Brook, NY 11794-5215, USA.

[2]Science and Technology Research Program, Smithtown High School East, St. James, NY 11780-1833, USA.

*These authors contributed equally to this work

‡Author for correspondence (david.matus@stonybrook.edu)

SUMMARY STATEMENT

Basement membrane invasion by the *C. elegans* anchor cell is coordinated by a dynamic gene regulatory network encompassing cell cycle dependent and independent sub-circuits.

ABSTRACT

Cellular invasion is a key part of development, immunity, and disease. Using the *in vivo* model of *C. elegans* anchor cell invasion, we characterize the gene regulatory network that promotes invasive differentiation. The anchor cell is initially specified in a stochastic cell fate decision mediated by Notch signaling. Previous research has identified four conserved transcription factors, *fos-1a* (Fos), *egl-43* (EVI1/MEL), *hlh-2* (E/Daughterless) and *nhr-67* (NR2E1/TLX), that mediate anchor cell specification and/or invasive differentiation. Connections between these transcription factors and the underlying cell biology that they regulate is poorly understood. Here, using genome editing and RNA interference, we examine transcription factor interactions prior to and after anchor cell specification. During invasion we identify that *egl-43*, *hlh-2*, and *nhr-67* function together in a type I coherent feed-forward loop with positive feedback. Conversely, prior to specification, these transcription factors function independent of one another to regulate LIN-12 (Notch) activity. Together, these results demonstrate that, although the same transcription factors can function in fate specification and differentiated cell behavior, a gene regulatory network can be rapidly re-wired to reinforce a post-mitotic, pro-invasive state.

Key words: EGL-43, FOS-1, HLH-2, NHR-67, gene regulatory network, cell invasion, cell cycle arrest

INTRODUCTION

Invasion through basement membranes (BM) is a cellular behavior that is integral to embryo placentation, tissue patterning during embryonic development, and immune response to infection and injury (Medwig and Matus, 2017; Rowe and Weiss, 2008). Increased cellular invasiveness is also a hallmark of metastatic cancer (Hanahan and Weinberg, 2011). Previous research has identified several cell-autonomous mechanisms that are highly conserved across different contexts of BM invasion (Kelley et al., 2014; Medwig and Matus, 2017). These include localization of F-actin and upregulation of matrix metalloproteinases (MMPs) to chemically degrade the BM (Hagedorn et al., 2009; Hagedorn et al., 2013; Kelley et al., 2019; Levitan and Greenwald, 1998; Morrissey et al., 2014; Sherwood et al., 2005). There is also growing evidence that cells must undergo cell cycle arrest in order to achieve invasive differentiation (Kohrman and Matus, 2017; Matus et al., 2015). How these tightly coordinated programs are transcriptionally regulated is not well understood.

As many contexts of cellular invasion occur deep within tissue layers and are thus difficult to visualize, we utilize morphogenesis of the *C. elegans* uterine-vulval connection as a genetically tractable and visually amenable model for examining cell invasion *in vivo* (Sherwood and Sternberg, 2003). During the mid-L3 stage, a

70 specialized uterine cell called the anchor cell (AC), invades the underlying BM,
71 connecting the uterus to the vulval epithelium to facilitate egg-laying (Fig. 1A,B)
72 (Sherwood and Sternberg, 2003). The AC itself is specified in a cell fate decision event
73 earlier in development, during the L2 stage, where two initially equipotent cells diverge
74 via stochastic Notch asymmetry, giving rise to the terminally differentiated AC and a
75 proliferative ventral uterine (VU) cell (Fig. 1A,B) (Wilkinson et al., 1994).
76
77 Prior research has identified four pro-invasive transcription factors (TFs) that function
78 cell autonomously to regulate AC invasion (Fig. 1A). These include the basic leucine
79 zipper TF *fos-1a* (Fos), the basic helix-loop-helix TF *hlh-2* (E/Daughterless), the nuclear
80 hormone receptor *nhr-67* (NR2E1/Tailless/TLX), and the zinc-finger TF *egl-43*
81 (EVI1/MEL) (Hwang et al., 2007; Matus et al., 2010; Rimann and Hajnal, 2007;
82 Schindler and Sherwood, 2011; Sherwood et al., 2005; Verghese et al., 2011). NHR-67
83 functions upstream of the cyclin dependent kinase inhibitor, CKI-1 (p21/p27), to induce
84 G1/G0 cell cycle arrest, which is necessary for AC invasion (Matus et al., 2015).
85 Independent of NHR-67 activity, FOS-1A regulates the expression of the long isoform of
86 *egl-43* (EGL-43L) and downstream effectors including multiple MMPs (*zmp-1, -3, and -*
87 *6*) and a cadherin (*cdh-3*) (Hwang et al., 2007; Kelley et al., 2019; Matus et al., 2010;
88 Rimann and Hajnal, 2007). HLH-2 independently regulates *cdh-3* along with other
89 targets and cytoskeletal polarity (Schindler and Sherwood, 2011). Prior work has also
90 suggested that EGL-43 and HLH-2 may regulate NHR-67 based on conserved HLH-2
91 binding motifs present in the *nhr-67* promoter as well as *egl-43* and *hlh-2* perturbation
92 experiments using *nhr-67* transcriptional and translational GFP reporters (Bodofsky et

93 al., 2018; Verghese et al., 2011). Interestingly, three of these TFs (*egl-43*, *hlh-2* and
94 *nhr-67*) also play key roles in the specification of the AC and VU cell fates during the L2
95 stage (Attner et al., 2019; Hwang et al., 2007; Karp and Greenwald, 2004; Sallee et al.,
96 2017; Verghese et al., 2011). How these four TFs function, independently and together,
97 to regulate both specification and invasive activity of the differentiated AC is poorly
98 understood.
99
100 Here, using new highly efficient RNA interference (RNAi) vectors (Sturm et al., 2018),
101 we identify novel roles for *egl-43* and *hlh-2*, in maintaining the AC in a cell cycle
102 arrested state. Additionally, we generated GFP knock-in alleles for each pro-invasive TF
103 by inserting GFP in-frame into each genomic locus using CRISPR/Cas9-mediated
104 genome engineering, allowing for quantitative measures of endogenous protein in the
105 context of native chromatin architecture and potential distal enhancer elements that may
106 be misrepresented using traditional transgenic reporters (Dickinson and Goldstein,
107 2016; Dickinson et al., 2013; Kim et al., 2014). Using these alleles, we report the onset
108 of relative expression of pro-invasive TFs in the lineages leading to the AC and dissect
109 their molecular epistatic interactions. We find that, prior to AC/VU specification, while all
110 four TFs regulate an endogenously tagged *lin-12*::GFP allele, none of the TFs regulate
111 each other. This network appears to be re-wired following specification, as we
112 characterized both a cell cycle independent circuit and a cell cycle dependent feed-
113 forward regulatory circuit with positive feedback critical for maintaining the AC in an
114 invasive, post-mitotic state. These findings provide new insights into how a set of

115 reiteratively used TFs can be re-purposed from regulating cell fate specification to
116 coordinating a differentiated cellular behavior.
117
118 **RESULTS**
119
120 ***Improved RNAi penetrance reveals novel phenotypes associated with depletion***
121 ***of pro-invasive TFs***
122
123 Our initial goal was to determine interactions between the four pro-invasive TFs, *fos-1*,
124 *egl-43*, *hlh-2* and *nhr-67*. To accomplish this, we first generated new RNAi targeting
125 constructs in the improved RNAi vector, T444T, which includes T7 termination
126 sequences to prevent the generation of non-specific RNA fragments from the vector
127 backbone, increasing the efficacy of gene silencing over the original RNAi targeting
128 vector, L4440 (Fig. S1A) (Sturm et al., 2018). As three of four pro-invasive TFs (*egl-43*,
129 *hlh-2* and *nhr-67*) also function during AC specification (Attner et al., 2019; Hwang et al.,
130 2007; Karp and Greenwald, 2004; Sallee et al., 2017; Verghese et al., 2011), we
131 assessed TF depletions in a genetic background where only the AC and neighboring
132 uterine cells are sensitive to RNAi following the AC/VU decision (Matus et al., 2010).
133 The uterine-specific RNAi sensitive strain was generated through tissue-specific
134 restoration of the RDE-1 Piwi/Argonaut protein in an *rde-1* mutant background using the
135 *fos-1a* promoter, which is expressed specifically in the somatic gonad during the late
136 L2/early L3 stage of larval development (Haerty et al., 2008; Hagedorn et al., 2009;
137 Matus et al., 2010; Matus et al., 2015). AC invasion was quantified as the presence or

138 absence of a BM gap, visualized by laminin::GFP, at the P6.p four-cell stage, a
139 developmental window where 100% of wild-type ACs are invaded (Fig. 1C, Table S1).
140 We also assessed invasion several hours later, following vulval morphogenesis,
141 allowing us to distinguish between delays in invasion and complete loss of invasive
142 capacity (Fig. 1E, Fig. S1D, Table S1). Depletion of each TF resulted in invasion defects
143 ranging from moderate penetrance (38%, *fos-1*) to highly penetrant (69-94%, *hlh-2*, *egl-*
144 *43*, and *nhr-67*), when synchronized L1-stage animals were plated on RNAi bacteria
145 and scored at the mid-L3 stage (P6.p 4-cell stage) and early L4 stage (P6.p 8-cell
146 stage) (Fig. 1C-E, Fig. S1D). Consistent with previous work, depletion of *fos-1* resulted
147 in single ACs that failed to breach the BM. Depletion of *nhr-67* resulted in proliferative,
148 non-invasive ACs at a high penetrance. Depletion of *egl-43* phenocopied *nhr-67*, with a
149 highly penetrant defect of multiple, non-invasive ACs. Lastly, depletion of *hlh-2* resulted
150 in pleiotropic phenotypes in the AC, from animals with zero, one, two or even several
151 cases of three or more ACs (Fig. 1D, S1C). In all cases, the penetrance of AC invasion
152 defects was significantly increased using a T444T-based RNAi targeting vector
153 compared to L4440-based vectors (Fig. S1A). Thus, use of the improved RNAi vector
154 revealed novel phenotypes resulting from depletion of *egl-43* and *hlh-2* during invasion,
155 phenocopying depletion of *nhr-67* resulting in multiple non-invasive ACs (Matus et al.,
156 2015).
157
158 Due to pleiotropy associated with *hlh-2* depletion, which affects AC specification and
159 invasion (Schindler and Sherwood, 2011), we sought to rule out that the extra *cdh-3-*
160 expressing ACs are due to defects in AC specification. Depletions using the traditional

161 RNAi vector, L4440, in the uterine-specific RNAi-sensitive background is sufficient to
162 bypass AC fate specification defects that occur in genetic backgrounds where all cells
163 are sensitive to RNAi (Matus et al., 2010). Specifically, loss of HLH-2 prior to AC
164 specification disrupts the *lin-12*(Notch)/*lag-2*(Delta)-dependent signaling cascade,
165 resulting in both pre-AC/VU cells adopting a VU fate, resulting in a zero AC phenotype.
166 During AC specification, loss of HLH-2 results in upregulation of pro-AC fate by
167 activating *lag-2*/Delta resulting in both AC/VU cells adopting an AC fate (Karp and
168 Greenwald, 2004; Schindler and Sherwood, 2011). Notably, *hlh-2* depletion using the
169 T444T vector resulted in a significantly greater occurrence of a zero AC phenotype as
170 compared to the L4440 *hlh-2* RNAi clone (Fig. 1D, S1A), suggesting that the enhanced
171 T444T vector may narrow the developmental window between restoration of RDE-1
172 function, the timing of the AC/VU decision and RNAi sensitivity. Thus, to bypass these
173 potential specification defects due to increased RNAi penetrance for *hlh-2* using the
174 T444T vector, we depleted *hlh-2* and the other TFs by RNAi using an L2-plating
175 strategy (Schindler et al. 2011), growing animals to the time of the L1/L2 molt on OP50
176 *E. coli* and then transferring them to TF-RNAi plates. L2 platings resulted in a lower
177 overall penetrance of AC invasion defects for all TF-RNAi treatments (Fig. S1B),
178 including *hlh-2* (43% at the P6.p 4-cell stage; Fig. 1D) but all animals possessed an AC.
179 Strikingly, some animals possessed multiple *cdh-3*-expressing ACs early (Fig. 1C),
180 while 10% of animals in the early L4 stage possessed multiple ACs (Fig. 1C-E, Fig.
181 S1C,D). As the number of ACs increased over developmental time (Fig. 1D-E), these
182 results suggest that the multiple ACs observed could be arising through loss of G1/G0-
183 cell cycle arrest and *nhr-67* activity (Matus et al., 2015).

184

185 ***Characterization of GFP-tagged alleles and RNAi penetrance***

186

187 Next, we sought to examine the relationship of these four TFs in the AC prior to and
188 during invasion by combining gene knockdown with endogenous GFP-tagged alleles.
189 To accomplish this, we used CRISPR/Cas9 genome editing technology to knock-in a
190 codon-optimized GFP tag into the endogenous locus of each TF (Fig. S2, Tables S4-6)
191 (Dickinson and Goldstein, 2016; Dickinson et al., 2013; Dickinson et al., 2015). First, we
192 examined a minimum of 50 L1/L2-stage animals to determine the onset of expression
193 for each TF in the somatic gonad, which is derived from two founder cells, Z1 and Z4
194 (Kimble and Hirsh, 1979). The two cells that can stochastically give rise to the AC are
195 the proximal great-granddaughters of Z1 and Z4 (Z1.ppp and Z4.aaa). Examination of
196 L1 and L2 stage somatic gonads revealed that *egl-43*::*GFP::egl-43* turns on first, in Z1
197 and Z4, and remains on in their descendants through the time of AC/VU specification
198 (Fig. 2A). As reported recently (Attner et al., 2019), *GFP::hlh-2* turns on at the second
199 division of Z1/Z4 cells in Z1.pp and Z4.aa. We also detected onset of *nhr-67::GFP* in
200 these cells in some animals, though it appears that their expression is weaker in
201 Z1.pp/Z4.aa as compared to *GFP::hlh-2*, but becomes robust in the AC/VU cells prior to
202 specification. Finally, we detected weak expression of *GFP::fos-1a* in L1 and L2 Z1/Z4
203 descendants that increased rapidly in the somatic gonad following AC specification (Fig.
204 2A). In summary, consistent with previously reported roles for *egl-43*, *hlh-2*, and *nhr-67*
205 in AC/VU specification (Hwang et al., 2007; Karp and Greenwald, 2004; Verghese et al.,
206 2011), we detect the presence of GFP in Z1/Z4 descendants.

207

208 Next, we examined the expression patterns of *TF::GFP* alleles following AC
209 specification. All four TFs showed robust GFP-localization in the AC nucleus prior to
210 and during invasion (Fig. 2B). Additionally, the GFP-tagged strains had similar
211 expression domains in the somatic gonad during the L3 larval stage as previously
212 reported by traditional multi-copy array transgenes (Hwang et al., 2007; Matus et al.,
213 2015; Rimann and Hajnal, 2007; Sherwood et al., 2005; Verghese et al., 2011). After
214 examining expression patterns, we then synchronized TF GFP-tagged strains and
215 collected a developmental time-course quantifying the expression of GFP-tagged
216 protein in the AC during uterine/vulval development (Fig 2B). All GFP-tagged TFs were
217 imaged using uniform acquisition settings on a spinning disk confocal using an EM-CCD
218 camera, allowing us to compare relative expression levels of endogenous GFP-tagged
219 proteins in the AC. Interestingly, all four TFs followed the same general trend in
220 expression levels, with a gradual increase in levels prior to invasion, peaking at or just
221 before the P6.p 4-cell stage when 100% of wild-type animals have generated a gap in
222 the BM. Expression levels then decreased following invasion, during vulval
223 morphogenesis, in the early L4 stage (P6.p 8-cell stage) (Fig. 2C).

224

225 As RNAi penetrance can be difficult to measure at single-cell level across a population
226 of animals, we next assessed the efficacy of our newly generated TF-RNAi vectors
227 quantitatively. To accomplish this, we first crossed a BM reporter (*laminin::GFP*) and an
228 AC marker (*cdh-3>mCherry:moeABD*; see Materials and Methods for transgene
229 nomenclature) into each endogenously GFP-tagged TF strain. We then performed a

230 series of RNAi depletion experiments targeting each TF and examining synchronized
231 animals at the P6.p 4-cell stage. As the insertion of GFP-tags into native genomic loci
232 can potentially interfere with gene function, we examined a minimum of 50 animals
233 treated with control (T444T) empty vector RNAi (Fig. 4). All four GFP-tagged strains
234 showed 100% BM breach at the normal time of invasion in control animals (empty
235 vector) (Fig. S3) and the animals all appear superficially wild-type. Additionally, all
236 alleles generated do not appear to affect viability or fertility. Although this does not rule
237 out other more subtle hypomorphic phenotypes, for the purpose of determining TF
238 regulatory relationships during AC invasion, we consider all alleles generated to be
239 equivalent to wild-type AC invasion.
240
241 Next, we examined a minimum of 50 animals following targeted TF-RNAi depletions,
242 collecting spinning disk confocal z-stacks using the same acquisition settings as used
243 for the developmental series (Fig. 2B) in all experiments. Following image quantification,
244 our results were consistent with the phenotypes identified in our original uterine-specific
245 RNAi screen (Fig. 1, S3). However, by being able to quantify depletion of endogenous
246 GFP-tagged TF targeted by RNAi, we were more accurately able to correlate phenotype
247 with mRNA depletion. The *nhr-67* and *egl-43* improved RNAi constructs strongly
248 knocked down their GFP-tagged endogenous targets, with depletions averaging 88%
249 and 75%, respectively (Fig. S3E). This strong knockdown of *nhr-67* and *egl-43* was also
250 correlated with highly penetrant AC invasion defects (61% and 100%, respectively). The
251 completely penetrant defect from *egl-43(RNAi)* segregated into 26% of animals
252 exhibiting a single AC that failed to invade and all other cases phenocopying loss of *nhr-*

253 *67*, with multiple *cdh-3*-expressing non-invasive ACs (Fig. S3E). Depletion of *GFP::fos-*
254 *1a* by RNAi was also highly penetrant, with a mean depletion of 92% of GFP-tagged
255 endogenous protein and 76% of treated animals had a defect in AC invasion (Fig. S3E).
256 Although only loss of *hlh-2* prior to AC specification can affect AC fate directly resulting
257 in zero ACs (Karp and Greenwald, 2004), *nhr-67* and *egl-43* also regulate the AC/VU
258 decision (Hwang et al., 2007; Verghese et al., 2011) . Thus, to ensure that the invasion
259 defects we were observing were the result of post-AC specification defects following TF
260 knockdown, we performed L2 platings and scored for invasion. Since L2 platings result
261 in less time (~12 hours at 25°C) exposed to TF-RNAi, we were not surprised to observe
262 a lower penetrance of AC invasion defects compared to L1 platings targeting the other
263 TFs (Fig. S3F). As all L2 platings phenocopied L1 platings, although at lower
264 penetrance and only depletion of *hlh-2* at the L1 stage directly affects AC fate, we
265 utilized L1 platings for their increased penetrance for *nhr-67*, *egl-43* and *fos-1* for the
266 remainder of our experiments. Together, these results suggest that following strong TF
267 depletion, loss of either *egl-43* or *hlh-2* phenocopy *nhr-67* depletion, generating multiple,
268 non-invasive ACs.
269
270 ***Identification of a feed-forward loop controlling NHR-67 activity***
271
272 Next, we examined the relationship between the four pro-invasive TFs during invasion.
273 To accomplish this, we performed a series of RNAi depletion experiments using
274 synchronized L1 or L2 (for *hlh-2*) stage animals and quantified the amount of GFP-
275 tagged endogenous TF in the AC in animals with defects in invasion at the P6.p four-

276 cell stage. While depletion of *fos-1* failed to significantly down-regulate levels of *nhr-*
277 *67::GFP,* depletion of *egl-43* resulted in a strong reduction (65%) of *nhr-67::GFP* in the
278 AC (Fig. 3A,B). Intriguingly, in animals with a single non-invasive AC following *hlh-*
279 *2(RNAi),* we saw only a partial reduction (19%) of *nhr-67::GFP* levels, while in animals
280 with multiple *cdh-3*-expressing cells we saw a significant reduction (49%) in *nhr-*
281 *67::GFP* (Fig. 5A,B). These results suggest that both *egl-43* and *hlh-2* co-regulate *nhr-*
282 *67* during invasion.
283
284 We repeated these TF-RNAi molecular epistasis experiments with the remaining three
285 TF-GFP-tagged strains and quantified depletion of GFP in animals with invasion
286 defects. Consistent with previous studies using transcriptional and translational
287 reporters (Hwang et al., 2007; Rimann and Hajnal, 2007), we found that depletion of
288 *fos-1* regulated levels of *egl-43::GFP::egl-43* (44% depletion) (Fig. 3C,D). No other TF
289 depletion significantly regulated the levels of *egl-43* in our experiments (Fig. 3C,D). *hlh-*
290 2 is predicted to regulate *egl*-43 activity based on the presence of two conserved E-box
291 binding motifs in the *egl-43* promoter (Hwang et al. 2007). However, we did not detect
292 regulation of *egl-43::GFP::egl-43* in either the AC (Fig. 3C,D) or neighboring ventral
293 uterine (VU) cells (Fig. S4). Next, we examined *GFP::hlh-2* levels following TF-RNAi
294 depletions. Intriguingly, we found a similar pattern of regulation based on AC
295 phenotype. Animals with single non-invasive ACs showed partial depletion of *GFP::hlh-*
296 *2* following *fos-1, egl-43,* or *nhr-67* depletion (35%, 20%, and 14%, respectively).
297 However, animals with multiple *cdh-3*-expressing ACs following *egl-43(RNAi)* or *nhr-*
298 *67(RNAi)* showed stronger depletion of *GFP::hlh-2* (66% and 73%, respectively) (Fig.

299 3E,F). Finally, we examined levels of *GFP::fos-1a* following TF depletions. Depletion of
300 either *nhr-67* or *egl-43* resulted in partial reduction of *GFP::fos-1a* levels in the AC (52%
301 and 49%, respectively) (Fig. 3G,H). Together, these results suggest that *egl-43*, *hlh-2*
302 and *nhr-67* may function together in a feed-forward regulatory loop with positive
303 feedback to maintain the AC in a post-mitotic, pro-invasive state.
304
305 ***Multiple ACs derive from proliferation***
306
307 As depletion of *egl-43* and *hlh-2* both regulate levels of *nhr-67* and their depletion
308 results in multiple ACs that fail to invade, we next wanted to assess whether their
309 depletion was functionally phenocopying depletion of *nhr-67*. To confirm that the
310 presence of multiple cells expressing the *cdh-3*-driven AC reporter were due to defects
311 in proliferation, we performed static imaging using a full-length translational *cdt-1*>CDT-
312 1::GFP reporter that indicates cell cycle progression (Fig. 4A). As CDT-1 must be
313 removed from origins of replication during DNA licensing, the transgene localizes to the
314 nucleus during G1/G0 and is largely cytosolic at the onset of S phase (Matus et al.,
315 2014; Matus et al., 2015). As expected, T444T (empty vector) and *fos-1(RNAi)* treated
316 animals consistently exhibited nuclear localization of CDT-1::GFP (Fig. 4A; 100%,
317 T444T, n = 15; 100%, *fos-1(RNAi),* n = 19 animals examined), indicating cell cycle
318 arrest. However, following depletion of *egl-43, hlh-2* and *nhr-67* we identified multiple
319 animals (Fig, 4A) possessing non-invasive ACs lacking nuclear CDT-1::GFP, indicative
320 of cycling ACs (67%, *egl-43(RNAi)*, n = 12/18; 58%, hlh-2(RNAi)L2 n = 11/19; 71%, nhr-
321 67(RNAi), n = 10/14 animals examined). Together, these results strongly support our

322 molecular epistasis data suggesting that *egl-43* and *hlh-2* function upstream of *nhr-67* to
323 maintain the post-mitotic state of the AC during invasion.
324
325 After examining the role of pro-invasive TFs in regulating cell cycle progression, we then
326 sought to examine other downstream targets involved in AC invasion. Using an
327 endogenously-tagged GFP reporter for the MMP, *zmp-1* (Kelley et al., 2019), we
328 assessed the ability of ACs to produce MMPs following *TF(RNAi)* depletion. We
329 confirmed previously published findings (Kelley et al., 2019; Sherwood et al., 2005) that
330 *fos-1* depletion results in reduction of *zmp-1* expression (Fig. 4B). Interestingly, in the
331 cases of the other *TF(RNAi)* treatments, a significant reduction of *zmp-1* expression
332 was only observed when multiple *cdh-3*-expressing ACs were present (Fig. 4B),
333 suggesting that cell cycle progression may downregulate production of MMPs.
334
335 ***EGL-43 and HLH-2 play roles in cell cycle dependent and independent pro-***
336 ***invasive pathways***
337
338 We have shown previously that the invasive activity of the AC following depletion of
339 NHR-67 can be completely rescued by restoring the AC to a post-mitotic G1/G0 state
340 through upregulation of the cyclin-dependent kinase inhibitor, CKI-1 (p21/p27) (Matus et
341 al., 2015). As our epistasis experiments revealed that *egl-43* and *hlh-2* positively co-
342 regulate NHR-67 activity, we induced AC-specific expression of CKI-1 using a *cdh-*
343 *3*>CKI-1::GFP integrated array and assessed invasion following RNAi depletions (Fig.
344 5A,B). As expected, induced expression of CKI-1::GFP in the AC completely rescued

345 *nhr-67(RNAi)* treated animals (Fig. 5A,B; 100% invaded (n = 42) as compared to 45% of
346 control animals lacking induced CKI-1::GFP (n = 62)). Additionally, *cdh-3*>CKI-1::GFP
347 partially rescued *hlh-2* depletion in L2 RNAi-feeding experiments by restoring AC
348 invasion in most animals examined (Fig. 5A,B; 87% invaded (n = 77), as compared to
349 56% of control animals (n = 59)). Inducing G1/G0 arrest in the AC failed to rescue *fos-*
350 *1(RNAi)* treated animals (Fig. 5A,B; 20% invaded (n = 35), as compared to 51% of
351 control animals (n = 53)). AC-specific expression of CKI-1::GFP blocked AC proliferation
352 following *egl-43(RNAi),* however this induced arrest failed to rescue invasion (Fig. 5A,B;
353 10% invaded (n = 31), as compared to 19% of control animals (n = 37)). This result
354 suggests that *egl-43* has pro-invasive functions outside of the cell cycle-dependent
355 pathway. In support of a role for *egl-43* outside of cell cycle control, induced CKI-1::GFP
356 restores the expression of a reporter of MMP activity (*zmp-1*>mCherry) in *nhr-67-*
357 depleted animals, but neither *fos-1* nor *egl*-43-depleted animals show restoration of
358 *zmp-1* transcription (Fig. 5C). Together, these results reveal the presence of two
359 integrated sub-circuits necessary for invasive activity, with *egl-43* and *hlh-2* likely having
360 a critical role for both circuits.
361
362 We next set out to test our putative network topology. To do this, we generated two new
363 single copy transgenic lines expressing either BFP-tagged codon optimized HLH-2 or
364 the genomic region of NHR-67, under the transcriptional control of a heat shock
365 promoter. Induced expression of HLH-2 failed to rescue AC invasion following depletion
366 of *egl-43*, *fos-1*, or *nhr-67*, consistent with *hlh-2* functioning upstream of *nhr-67* and the
367 cell cycle independent roles of *egl-43* and *fos-1* in regulating AC invasion (Fig. S5A).

368 Similarly, induced expression of NHR-67 did not rescue invasion in *egl-43(RNAi)* and
369 *fos-1(RNAi)* treated animals (Fig. S5B). Furthermore, induced expression of NHR-67
370 failed to rescue AC invasion in *hlh-2(RNAi)* treated animals (Fig. S5B). This result,
371 paired with the prevalence of single non-invasive ACs (Fig. 1C) and only partial rescue
372 from induced CKI-1 (Fig. 5A,B) suggest that *hlh-2* regulates invasive targets
373 independent of its role in regulating *nhr-67* and cell cycle arrest.
374
375 As our induced TF experiments failed to rescue invasion defects, we examined an *nhr-*
376 *67* hypomorphic allele (*nhr-67(pf88))*, which we have previously shown results in an
377 incomplete penetrance of mitotic, non-invasive ACs (Matus et al., 2015). Notably, *nhr-*
378 *67(RNAi)* using the enhanced T444T vector did not significantly increase the invasion
379 defect of the hypomorphic allele (Fig. S6), supporting previous results using the L4440-
380 based *nhr-67* RNAi vector (Matus et al., 2015). Thus, the *nhr-67(pf88)* allele may
381 represent a putative null phenotype for AC invasion. Similar to our results with *nhr-*
382 *67(RNAi)*, depletion of *hlh-2* also failed to significantly enhance the *nhr-67(pf88)* AC
383 invasion defect (Fig. S6). Together, these results suggest that *hlh-2* functions upstream
384 of *nhr-67* in maintaining the AC in a post-mitotic, pro-invasive state.
385
386 ***EGL-43 isoforms function redundantly and in an autoregulative manner during***
387 ***AC invasion***
388
389 Two functional isoforms of *egl-43* are encoded in the *C. elegans* genome (Fig. S7A).
390 Previous research has suggested that the longer isoform functions downstream of *fos-*

391 *1a* to modulate MMP expression and other *fos-1* transcriptional targets, including *cdh-3*
392 (Hwang et al., 2007; Rimann and Hajnal, 2007). The shorter isoform has been predicted
393 to either function in Notch/Delta-mediated AC specification (Hwang et al., 2007) and
394 later Notch/Delta-mediated patterning of the ventral uterus (Hwang et al., 2007) or as a
395 potential competitive inhibitor for long isoform binding of downstream targets (Rimann
396 and Hajnal, 2007). Additionally, *fos-1a* and *egl-43* have been shown to function in an
397 incoherent feed-forward loop with negative feedback, with *fos-1a* positively regulating
398 and *egl-43* negatively regulating the levels of *mig-10*/lamellipodin, a key adhesion
399 protein important for stabilizing the attachment of the AC to the BM (Wang et al., 2014).
400 Titrating levels of MIG-10 is critical, as overexpression of MIG-10 results in AC invasion
401 defects (Wang et al., 2014). Although it is readily apparent that levels of EGL-43 are
402 also important, it is unclear from previous studies whether the two isoforms have
403 divergent functions during invasion. Thus, we next decided to explore *egl-43* isoform
404 function.
405
406 First, we were generated a knock-in allele of GFP at the *egl-43* N-terminus to
407 specifically tag the long isoform *(GFP::egl-43L*). This allowed us to compare expression
408 patterns of the long isoform to the internally GFP-tagged allele that should dually label
409 both isoforms (Fig. S7A,B). We examined animals during uterine-vulval development
410 and found overlapping expression patterns between both isoforms with strong
411 AC/VU/DU expression in the somatic gonad (Fig. S7B). Next, we generated an *egl-43L*-
412 specific improved RNAi targeting vector in T444T and examined *egl-43L* depletion in the
413 uterine-specific RNAi sensitive genetic background (Hagedorn et al., 2009; Matus et al.,

414 2010). Depletion of *egl-43L* resulted in a penetrant AC invasion defect, as expected, but
415 notably, we detected the presence of animals with both a single non-invasive AC (19%)
416 and animals with multiple ACs (39%) (Fig. 6A,B), similar to depletion of both isoforms
417 (Fig. 1C,E). We then assessed if the long isoform has the same quantitative relationship
418 to the other TFs as observed when targeting both isoforms. Indeed, *egl-43(RNAi)* and
419 *egl-43L(RNAi)* exhibited comparable levels of depletion of *egl-43::GFP::egl-43* (75%,
420 78%), *GFP::hlh-2* (66%, 60%), and *nhr-67::GFP* (66%, 64%, respectively) ($n \geq 25$
421 animals examined per treatment) (Fig. S7C).
422
423 By using the self-excising cassette (SEC) method (Dickinson et al. 2016) to generate
424 GFP knock-in alleles, prior to Cre-Lox recombination, the insertion of GFP at the N-
425 terminus of a locus with a ~6kb SEC generates a transcriptional reporter at the
426 endogenous locus. Additionally, this ~6kb DNA cassette also often interferes with the
427 native transcriptional machinery at the locus where it is inserted, generating a strong
428 loss-of-function or putative null allele (Dickinson and Goldstein, 2016). To determine if
429 newly generated alleles exhibit loss-of-function phenotypes and to examine
430 transcriptional output, we next examined the pre-floxed versions of both edited knock-in
431 alleles of *egl-43*, in the presence of an mT1 balancer, as homozygous animals are non-
432 fertile. Similar to the putative null allele, *egl-43(tm1802 (*Rimann and Hajnal, 2007), the
433 allele resulting from the SEC insertion of the internal GFP-tag had an extremely low
434 frequency of escapers, and we were unable to obtain L3-stage animals to examine for
435 AC invasion defects. However, similar to our results with RNAi (Fig. 6A,B), an allele
436 resulting from SEC insertion with the long isoform (*egl-43(bmd135)*) displayed a 31%

437 AC invasion defect (n = 11/36), with animals containing either single or multiple non-
438 invading ACs (Fig. S7D,E). Finally, as previous reports based on transgenic
439 transcriptional reporters have suggested that *egl-43* may be autoregulatory (Matus et
440 al., 2010; Rimann and Hajnal, 2007; Wang et al., 2014), we examined the mT1-
441 balanced pre-floxed allele of the internally-tagged *egl-43* targeting both isoforms (*egl-*
442 *43::GFP^SEC^::egl-43*). In support of these previous studies we found strong evidence
443 of autoregulation at the endogenous locus, as *egl-43(RNAi)* reduced the expression of
444 GFP by 65% (n ≥ 25 animals) (Fig. 6C,D). Taken together, these results suggest that
445 both isoforms of *egl-43* function redundantly to regulate multiple transcriptional sub-
446 circuits critical for invasion.
447
448 ***Activation of the pro-invasive gene regulatory network (GRN) occurs post-***
449 ***specification***
450
451 Our results here identify a putative feed-forward loop between *egl-43*, *hlh-2* and *nhr-67*
452 to maintain levels of NHR-67, that we have previously shown is critical for keeping the
453 AC in a post-mitotic, pro-invasive state (Matus et al. 2015). As these same TFs also
454 have been shown to function during the AC/VU decision (Hwang et al., 2007; Karp and
455 Greenwald, 2004; Verghese et al., 2011) we examined if the same regulatory
456 relationships were utilized during cell fate specification and differentiation. Intriguingly,
457 our examination of TF onset establishes a hierarchy of *egl-43*, *hlh-2*, and *nhr-67*
458 reaching steady-state levels in the descendants of Z1 and Z4, although all three TFs are
459 robustly expressed in the AC/VU cells (Fig. 2A). To examine TF regulatory relationships

460 prior to specification, we performed L1 TF RNAi platings and examined expression
461 levels of TF-GFP in the AC/VU cells in L2 stage animals. While each TF RNAi robustly
462 depleted its target GFP allele, we failed to detect any molecular epistatic interactions
463 between TFs in the AC/VU cells (Fig. 7A,B). In support of previous research
464 demonstrating a role for these TFs in regulating the AC/VU decision (Hwang et al.,
465 2007; Karp and Greenwald, 2004; Verghese et al., 2011), we detected significant
466 depletion of an endogenously GFP-tagged allele of *lin-12* (Notch) (Fig. 7C,D). Together,
467 these results suggest that despite the re-iterative use of the same set of TFs in
468 specification and invasion, the GRN we characterize here is specific for the post-
469 specification pro-invasive behavior of the AC.
470
471
472 **DISCUSSION**
473
474 Cellular invasion requires coordination of extrinsic cues from the surrounding
475 microenvironment and orchestration of intrinsic regulatory circuits (Rowe and Weiss,
476 2008; Sherwood and Plastino, 2018). We focus here on exploring the intrinsic pathways
477 that autonomously regulate *C. elegans* AC invasion. Combining improved RNAi
478 targeting vectors with GFP-tagged alleles enabled us to correlate phenotype to
479 depletion of the endogenous mRNAs and compare regulatory relationships in a
480 quantitative framework. Our experiments reveal new roles for *egl-43* and *hlh-2* in
481 regulating *nhr-67*-mediated cell cycle arrest and suggest that these TFs function in a
482 coherent feed-forward loop with positive feedback. Additionally, we confirm previous

work demonstrating that *egl-43* is autoregulatory and demonstrate that it functions in both cell cycle-dependent and independent sub-circuits to orchestrate invasion (Fig. 8). Together, building upon previous work using transgenic approaches (Bodofsky et al., 2018; Hwang et al., 2007; Rimann and Hajnal, 2007; Schindler and Sherwood, 2011; Verghese et al., 2011), our results using endogenously tagged alleles provide the first description of the native regulatory relationships between the four TFs that promote invasive differentiation during *C. elegans* uterine-vulval attachment.

A key function of *nhr-67* is to maintain the post-mitotic state of the AC (Matus et al., 2015). Here, we demonstrate that *egl-43* and *hlh-2* both regulate *nhr-67*, and that *nhr-67*-depletion also reduces HLH-2 levels. Network inference suggests these three TFs function in a classic type I coherent feed-forward loop regulatory circuit with positive feedback (Mangan and Alon, 2003) (Fig. 8). Our model fits with data by others showing that *hlh-2* may directly bind to the *nhr-67* promoter through two canonical E-box motifs found in a 164 bp window in a functional promoter element deleted in several hypomorphic alleles of *nhr-67* (Bodofsky et al., 2018; Matus et al., 2015; Verghese et al., 2011). Further, deletion of these *hlh-2* conserved binding sites results in loss of AC-specific GFP expression in transgenic lines (Bodofsky et al., 2018). While others have also reported positive regulation by EGL-43 on *nhr-67* activity via transgenic reporters (Bodofsky et al., 2018), this interaction, and many of the others TF interactions, may be indirect, as no known binding sites exist for EGL-43 in the *nhr-67* promoter. Alternatively, EGL-43 and NHR-67 have been predicted, based on yeast two-hybrid experiments, to interact at the protein-protein level (Reece-Hoyes et al., 2013).

506

507 We have also examined the activity of the two previously identified isoforms of *egl-43*
508 (Hwang et al., 2007; Rimann and Hajnal, 2007). As both mutant analyses and RNAi
509 depletion of the long isoform phenocopy depletion of both isoforms, our data suggest
510 that either the long isoform of *egl-43* functions redundantly with the short isoform or that
511 it functions as the dominant isoform at the intersection of multiple regulatory circuits. Of
512 the these two possible hypotheses, the latter is supported by a recent report
513 demonstrating that the long isoform of *egl-43* is a key upstream regulator of the post-
514 mitotic state of the AC as mutation of the transcriptional start methionine of the short
515 isoform of *egl-43* has no observable AC invasion defect and an AC-specific genetic
516 knockout of the long isoform results in mitotic, non-invasive ACs (Deng et al., 2019).
517

518 Together, our data and corroborating evidence from the literature support the existence
519 of a coherent feed-forward circuit with positive feedback among *egl-43*, *hlh-2* and *nhr-*
520 *67,* in maintaining the post-mitotic state of the AC (Fig. 8). We have previously shown
521 that *nhr-67* positively regulates transcripts of *cki-1* specifically in the AC (Matus et al.,
522 2015). Thus, to test our putative regulatory circuit, we induced expression of *cki-1* in the
523 AC, which prevents the AC from inappropriately entering the cell cycle. This forced
524 G1/G0 arrest fully rescues *nhr-67* depletion (Matus et al., 2015). Induced *cki-1* partially
525 rescued *hlh-2* depletion but failed to rescue *egl-43* depletion. Heat shock induced
526 expression of *nhr-67* failed to rescue either *hlh-2* or *egl-43*, suggesting that *hlh-2*, like
527 *egl-43*, has a cell cycle-independent function. These results suggest that *egl-43* and *hlh-*
528 *2* function in multiple regulatory circuits. For *egl-43*, this is supported by recent work

529 demonstrating a type I incoherent feed-forward loop between *fos-1a, egl-43L* and the
530 BM adhesion protein MIG-10/lamellipodin (Wang et al., 2014). Finally, our observation
531 that *egl-43* is autoregulatory, also shown previously by *promoter*>GFP fusion
532 experiments (Matus et al., 2015; Rimann and Hajnal, 2007; Wang et al., 2014) supports
533 a model where *egl-43* occupies a key node at the intersection of multiple pro-invasive
534 circuits (Fig. 8).
535
536 Feed-forward regulatory loops are likely the most well described network motif occurring
537 in all GRNs (Cordero and Hogeweg, 2006; Davidson, 2010; Mangan and Alon, 2003).
538 From *E. coli* (Milo et al., 2002; Shen-Orr et al., 2002) and yeast (Lee et al., 2002; Milo et
539 al., 2002) to a myriad of examples across the Metazoa (reviewed in Davidson, 2010),
540 feed-forward loops are thought to function as filters for transient inputs (reviewed in
541 Alon, 2007; Hinman, 2016). The addition of positive feedback, generating a coherent
542 feed-forward loop, provides stability to a sub-circuit and is often found in differentiation
543 gene batteries coincident with autoregulation (Davidson, 2010). These network motifs
544 have been described in many developmental contexts, from MyoD-driven vertebrate
545 skeletal muscle differentiation (Penn et al., 2004), the patterning of the Drosophila egg
546 shell via the TF Broad and interactions with EGFR and Dpp signaling (Yakoby et al.,
547 2007), Pax6-dependent regulation of c-Maf and crystallin expression in the mouse
548 embryonic lens (Xie and Cvekl, 2011) and terminal selector neuronal differentiation in *C.*
549 *elegans* and mammals (reviewed in Hobert, 2008). During *C. elegans* embryonic
550 development, a series of coherent feed-forward loops utilizing SKN-1/MED-1,2 and then
551 a suite of reiteratively used GATA factors (END-1,-3) are required to successfully

552 pattern endomesoderm development (reviewed in Maduro, 2009). Thus, our
553 identification of a coherent feed-forward loop in the *C. elegans* AC maintaining the post-
554 mitotic state, likely evolved to coordinate AC cell cycle exit, both as a by-product of
555 terminal differentiation and a morphogenetic requirement for invasive behavior (Matus
556 et al., 2015). AC invasion is necessary for egg-laying, and defects in the process results
557 in penetrant Protruding vulva/Egg-laying defective (Pvl/Egl) phenotypes, reducing
558 fecundity in individual animals by nearly ten-fold. Thus, redundant control of the sub-
559 circuit regulating differentiation and cell cycle arrest may have been under strong
560 selection, providing an explanation for the regulatory relationships between *egl-43*, *hlh-2*
561 and *nhr-67* we characterize here.
562
563 As *egl-43*, *hlh-2* and *nhr-67* reach steady state levels prior to the time of AC/VU
564 specification and individually have been previously shown to regulate different aspects
565 of the stochastic cell fate decision between the AC and VU (Hwang et al., 2007; Karp
566 and Greenwald, 2004; Verghese et al., 2011), we performed RNAi depletion
567 experiments and examined TF::GFP levels in the AC/VU cells during the L2 stage.
568 Surprisingly, we found no evidence of regulation between the TFs at this stage, though
569 as expected, all three TFs regulated levels of endogenously tagged *lin-12::GFP* (Notch).
570 This suggests that the feed forward loop functions specifically in the post-specification
571 AC to maintain the post-mitotic, invasive state (Fig. 8). One plausible explanation for
572 this change in network topology between specification and differentiation is that
573 coordination between chromatin remodeling and TF activity likely changes the genomic
574 landscape between the bipotential AC/VU cells and the post-mitotic, differentiated AC.

575 Additionally, there may be differentially expressed co-factor(s) functioning during
576 specification or invasion that facilitate interactions between TFs. Reiterative use of the
577 same TFs to program different cell behaviors has been examined during neuronal
578 differentiation (Guillemot, 2007) and neural crest specification and migration, as the
579 winged-helix TF FoxD3 was recently shown to regulate multiple independent chromatin-
580 organizing circuits, functioning as a pioneer factor during zebrafish neural crest
581 specification and a transcriptional repressor during later events, including EMT and
582 migration (Lukoseviciute et al., 2018). Whether or not *egl-43*, *nhr-67* or *hlh-2* function as
583 pioneer factors during AC/VU specification is an open question, and one will soon be
584 tractable through FACS isolation and the application of newer next-generation
585 sequencing tools such as ATAC-seq (Assay for Transposase-Accessible Chromatin
586 using sequencing) or CUT&RUN (Cleavage Under Targets and Release Using
587 Nuclease) (Skene and Henikoff, 2017).
588
589 We are just beginning to understand connections between regulatory circuits and
590 morphogenetic behaviors (Christiaen et al., 2008; Martik and McClay, 2015; Saunders
591 and McClay, 2014). It is our hope that the ease of genome editing and protein
592 perturbation strategies will facilitate the kind of analyses we have performed here in
593 other metazoan systems. In summary, in this study we characterize the complex
594 relationships between the four pro-invasive TFs that function during AC differentiation to
595 program invasive behavior. We show that although the TFs are reiteratively used in both
596 cell fate specification and in a differentiated cell behavior, invasion, that the network
597 topology is rewired following specification. We identify a classic type I feed forward loop

598 regulating mitotic exit and controlling a switch between proliferative and invasive
599 behavior. Whether or not similar circuit architecture is utilized to regulate invasive and
600 proliferative cell biology in other developmental invasive contexts, including mammalian
601 trophoblast implantation and placentation (Carter et al., 2015; Red-Horse et al., 2004)
602 and epithelial to mesenchymal transition events during gastrulation (Vega et al., 2004)
603 is still poorly understood. Finally, as there appear to be many cancer sub-types that may
604 switch between proliferative and invasive fates (reviewed in Kohrman and Matus, 2017),
605 improving our understanding of the transcriptional network architecture of invasive cells
606 may provide new therapeutic nodes to target in reducing the lethality associated with
607 cancer metastasis.
608

609 **MATERIALS AND METHODS**

610

611 ***C. elegans strains and culture conditions***

612

613 Animals were reared under standard conditions and cultured at 25°C, with the exception
614 of temperature-sensitive strains including those containing heat shock inducible
615 transgenes or the *rrf-3(pk1426)* allele (conferring RNAi hypersensitivity), which were
616 maintained at 15°C and 20°C (Brenner, 1974; Simmer et al., 2002). Heat shock
617 inducible transgenes were activated by incubating animals on plates at 32°C for 1 hour
618 following AC specification and again just prior to AC invasion. Animals were
619 synchronized for experiments through alkaline hypochlorite treatment of gravid adults to
620 isolate eggs (Porta-de-la-Riva et al., 2012). In the text and figures, we designate linkage

621 to a promoter through the use of the (>) symbol and fusion of a proteins via a (::)
622 annotation. The following transgenes and alleles were used in this study: *qyIs102[fos-*
623 *1>RDE-1;myo-2>YFP]* **LG I** *hlh-2(bmd90[hlh-2>LoxP::GFP::HLH-2]), qyIs227[cdh-*
624 *3>mCherry::moeABD], bmd121[LoxP::hsp>NHR-67::2xBFP], bmd142[hsp>HLH-*
625 *2::2xBFP];* **LG II** *egl-43(bmd87[egl-43>SEC::GFP::EGL-43]), egl-43(bmd88[egl-*
626 *43>LoxP::GFP::EGL-43]), egl-43(bmd136[egl-43L>LoxP::GFP::EGL-43]) rrf-3(pk1426);*
627 *qyIs17 [zmp-1>mCherry*] **LG III** *unc-119(ed4),* **LG IV** *nhr-67(syb509[nhr-67>NHR-*
628 *67::GFP]), qyIs10[lam-1>LAM-1::GFP]* **LG V** *fos-1(bmd138[fos-1>LoxP::GFP::FOS-1]),*
629 *qyIs225[cdh-3>mCherry::moeABD], rde-1(ne219), qyIs24[cdh-3$^{1.5}$>mCherry::PLCδPH],*
630 *qyIs266[cdh-3>CKI-1::GFP]* **LG X** *qyIs7[lam-1>LAM-1::GFP]*. See Table S3 for
631 additional details of strains used and generated in this study.
632
633 ***Molecular biology and microinjection***
634
635 Transcription factors were tagged at their endogenous loci using CRISPR/Cas9 genome
636 editing via microinjection into the hermaphrodite gonad (Dickinson and Goldstein, 2016;
637 Dickinson et al., 2013). Repair templates were generated as synthetic DNAs from either
638 Integrated DNA Technologies (IDT) as gBlocks or Twist Biosciences as DNA fragments
639 and cloned into *ccdB* compatible sites in pDD282 by New England Biolabs Gibson
640 assembly (Dickinson et al., 2015). Homology arms ranged from 690-1200 bp (see
641 Tables S4-6 for additional details). sgRNAs were constructed by EcoRV and NheI
642 digestion of the plasmid pDD122. A 230 bp amplicon was generated replacing the
643 sgRNA targeting sequence from pDD122 with a new sgRNA and NEB Gibson assembly

644 was used to generate new sgRNA plasmids (see Tables S4-6 for additional details).
645 Hermaphrodite adults were co-injected with guide plasmid (50 ng/μL), repair plasmid
646 (50 ng/μL), and an extrachromosomal array marker (pCFJ90, 2.5 ng/μL), and incubated
647 at 25 ºC for several days before carrying out screening and floxing protocols associated
648 with the SEC system (Dickinson et al., 2015).
649
650 ***RNA interference***
651
652 An RNAi library of the pro-invasive TFs was constructed by cloning 950-1000 bp of
653 synthetic DNA (663 bp for the *egl-43* long-specific isoform) based on cDNA sequences
654 available on WormBase (www.wormbase.org) into the highly efficient T444T RNAi
655 vector (Grove et al., 2018; Sturm et al., 2018). Synthetic DNAs were generated by IDT
656 as gBlocks or Twist Biosciences as DNA fragments and cloned into restriction digested
657 T444T using NEB Gibson Assembly (see Tables S4-5,7 for additional details). For most
658 experiments, synchronized L1 stage animals were directly exposed to RNAi through
659 feeding with bacteria expressing dsRNA (Conte Jr. et al., 2015). Due to the fact that
660 early *hlh-2* RNAi treatment perturbs AC specification, animals were initially placed on
661 empty vector RNAi plates and then transferred to *hlh-2* RNAi plates following AC
662 specification, approximately 12 hours later at 25°C or 24 hours later at 15°C (Schindler
663 and Sherwood, 2011).
664
665 ***Live cell imaging***
666

667 All micrographs included in this manuscript were collected on a Hamamatsu Orca EM-
668 CCD camera mounted on an upright Zeiss AxioImager A2 with a Borealis-modified
669 CSU10 Yokagawa spinning disk scan head using 488 nm and 561 nm Vortran lasers in
670 a VersaLase merge and a Plan-Apochromat 100x/1.4 (NA) Oil DIC objective.
671 MetaMorph software (Molecular Devices) was used for microscopy automation. Several
672 experiments were scored using epifluorescence visualized on a Zeiss Axiocam MRM
673 camera, also mounted on an upright Zeiss AxioImager A2 and a Plan-Apochromat
674 100x/1.4 (NA) Oil DIC objective. Animals were mounted into a drop of M9 on a 5%
675 Noble agar pad containing approximately 10 mM sodium azide anesthetic and topped
676 with a coverslip.
677
678 ***Scoring of AC invasion***
679
680 AC invasion was scored at the P6.p 4-cell stage, when 100% of wild-type animals
681 exhibit a breached BM (Sherwood and Sternberg, 2003). Presence of green
682 fluorescence under the AC, in strains with the laminin::GFP transgene, or presence of a
683 phase dense line, in strains without the transgene, was used to assess invasion. Wild-
684 type invasion is defined as a breach as wide as the basolateral surface of the AC,
685 whereas partial invasion indicates the presence of a breach smaller than the footprint of
686 the AC (Sherwood and Sternberg, 2003). Raw scoring data is available in Tables S1-2.
687
688 ***Image quantification and statistical analyses***
689

690 Images were processed using FIJI/ImageJ (v.1.52q) (Schindelin et al., 2012).
691 Expression levels of TFs were quantified by measuring the mean gray value of AC
692 nuclei, defined as somatic gonad cells strongly expressing the *cdh-*
693 *3*>mCherry::moeABD transgene, subtracted by the mean gray value of a background
694 region of equal area to account for EM-CCD camera noise, which we use as a proxy for
695 background fluorescence, as measurements of the mean grey value of unlabeled ACs
696 approximately correspond to camera noise (means = 2514.2 and 2243.5, respectively).
697 Levels of *zmp-1*>mCherry were quantified in control and *cdh-3*>CKI-1::GFP animals by
698 measuring the mean gray value of the entire AC, selected either by a hand drawn
699 region of interest or using the threshold and wand tools in FIJI/ImageJ. For
700 characterization of downstream targets (Fig. 4) and molecular epistasis experiments
701 (Fig. 3, S3 & S7) at the L3 stage, only animals TF-RNAi exhibiting defects in invasion
702 were included in the analysis. Data was normalized to negative control (empty vector)
703 values for the plots in Fig. 3-7, S5-6, & S7, and to both negative control and positive
704 control values for determining the interaction strengths represented in Fig. 8. Images
705 were overlaid and figures were assembled using Adobe Photoshop (v. 20.0.6) and
706 Illustrator CS (v. 10.14), respectively. Statistical analyses and plotting of data were
707 conducted using RStudio (v. 1.1.463). Individual data points for each experiment were
708 collected over multiple days. Statistical significance was determined using either a two-
709 tailed Student's t-test or Fisher's exact probability test. Figure legends specify when
710 each test was used and the p-value cut-off set.
711

712 **ACKNOWLEDGMENTS**

We are grateful to R. Adikes, B. Kinney, A. Kohrman, M. Martinez and B. Martin for comments on the manuscript. We also thank I. Greenwald for providing the endogenously-tagged *lin-12*>LIN-12::GFP strain used in Fig. 7C.

COMPETING INTERESTS

No competing interests declared.

AUTHOR CONTRIBUTIONS

D.Q.M., T.N.M., and J.J.S. designed the experiments. All authors performed the experiments. T.N.M. and D.Q.M. performed the data analyses and wrote the paper with feedback from the other authors.

FUNDING

This work was funded by the National Institute of Health (NIH) National Cancer Institute [5R00CA154870-05 to D.Q.M.] and National Institute of General Medical Sciences (NIGMS) [1R01GM121597-01 to D.Q.M.]. D.Q.M. is also a Damon Runyon-Rachleff Innovator supported (in part) by the Damon Runyon Cancer Research Foundation [DRR-47-17]. T.N.M. is supported by the NIH Eunice Kennedy Shriver National Institute of Child Health and Human Development [F31HD100091-01]. J.J.S. is supported by NIGMS [3R01GM121597-02S1] and N.J.P. is supported by the American Cancer Society [132969-PF-18-226-01-CSM]. Some strains were provided by the *Caenorhabditis* Genetics Center, which is funded by the NIH Office of Research Infrastructure Programs [P40 OD010440].

REFERENCES

Alon, U. (2007). Network motifs: theory and experimental approaches. *Nat. Rev. Genet.* **8**, 450–61.

Attner, M. A., Keil, W., Benavidez, J. M. and Greenwald, I. (2019). HLH-2/E2A Expression Links Stochastic and Deterministic Elements of a Cell Fate Decision during C. elegans Gonadogenesis. *Curr. Biol.* **29**, 1–7.

Bodofsky, S., Liberatore, K., Pioppo, L., Lapadula, D., Thompson, L., Birnbaum, S., McClung, G., Kartik, A., Clever, S. and Wightman, B. (2018). A tissue-specific enhancer of the C. elegans nhr-67/tailless gene drives coordinated expression in uterine stem cells and the differentiated anchor cell. *Gene Expr. Patterns* **30**, 71–81.

Brenner, S. (1974). The genetics of *Caenorabditis elegans*. *Genetics* **77**, 71–94.

Carter, A. M., Enders, A. C. and Pijnenborg, R. (2015). The role of invasive trophoblast in implantation and placentation of primates. *Philos. Trans. R. Soc. B Biol. Sci.* **370**, 20140070–20140070.

Christiaen, L., Davidson, B., Kawashima, T., Powell, W., Nolla, H., Vranizan, K. and Levine, M. (2008). The transcription/migration interface in heart precursors of Ciona intestinalis. *Science (80-.).* **320**, 1349–1352.

Conte Jr., D., T. Macneil, L., J. M. Walhout, A. and C. Mello, C. (2015). *RNA Interference in Caenorhabditis Elegans*.

Cordero, O. X. and Hogeweg, P. (2006). Feed-forward loop circuits as a side effect of genome evolution. *Mol. Biol. Evol.* **23**, 1931–1936.

Davidson, E. H. (2010). Emerging properties of animal gene regulatory networks. *Nature* **468**, 911–920.

Deng, T., Daube, M., Hajnal, A. and Lattmann, E. (2019). The C. elegans homolog of the Evi1 proto-oncogene, egl-43, coordinates G1 cell cycle arrest with pro-invasive gene expression during anchor cell invasion. *bioRxiv* 1–37.

Dickinson, D. J. and Goldstein, B. (2016). CRISPR-based methods for caenorhabditis elegans genome engineering. *Genetics* **202**, 885–901.

Dickinson, D. J., Ward, J. D., Reiner, D. J. and Goldstein, B. (2013). Engineering the Caenorhabditis elegans genome using Cas9-triggered homologous recombination. *Nat. Methods* **10**, 1028–1034.

Dickinson, D. J., Pani, A. M., Heppert, J. K., Higgins, C. D. and Goldstein, B. (2015). Streamlined genome engineering with a self-excising drug selection cassette. *Genetics* **200**, 1035–1049.

Grove, C., Cain, S., Chen, W. J., Davis, P., Harris, T., Howe, K., Kishore, R., Lee, R., Paulini, M., Raciti, D., et al. (2018). Using WormBase, a genome biology resource for Caenorhabditis elegans and related nematodes. *Methods Mol. Biol.* **1757**, 399–470.

Guillemot, F. (2007). Spatial and temporal specification of neural fates by transcription factor codes. *Development* **134**, 3771–3780.

Haerty, W., Artieri, C., Khezri, N., Singh, R. S. and Gupta, B. P. (2008). Comparative analysis of function and interaction of transcription factors in nematodes: Extensive conservation of orthology coupled to rapid sequence evolution. *BMC Genomics* **9**, 1–16.

Hagedorn, E. J., Yashiro, H., Ziel, J. W., Ihara, S., Wang, Z. and Sherwood, D. R. (2009). Integrin Acts Upstream of Netrin Signaling to Regulate Formation of the Anchor Cell's Invasive Membrane in C. elegans. *Dev. Cell* **17**, 187–198.

Hagedorn, E. J., Ziel, J. W., Morrissey, M. A., Linden, L. M., Wang, Z., Chi, Q., Johnson, S. A. and Sherwood, D. R. (2013). The netrin receptor DCC focuses invadopodia-driven basement membrane transmigration in vivo. *J. Cell Biol.* **201**, 903–913.

Hanahan, D. and Weinberg, R. A. (2011). Hallmarks of cancer: The next generation. *Cell* **144**, 646–674.

Hinman, V. F. (2016). Gene Networks Driving Development, Conservation and Evolution of. *Encycl. Evol. Biol.* 110–116.

Hobert, O. (2008). Regulatory logic of neuronal diversity: Terminal selector genes and selector motifs. *Proc. Natl. Acad. Sci.* **105**, 20067–20071.

Hwang, B. J., Meruelo, A. D. and Sternberg, P. W. (2007). C. elegans EVI1 proto-oncogene, EGL-43, is necessary for Notch-mediated cell fate specification and regulates cell invasion. *Development* **134**, 669–679.

Karp, X. and Greenwald, I. (2004). Multiple roles for the E/Daughterless ortholog HLH-2 during C. elegans gonadogenesis. *Dev. Biol.* **272**, 460–469.

Kelley, L. C., Lohmer, L. L., Hagedorn, E. J. and Sherwood, D. R. (2014). Traversing the basement membrane in vivo: A diversity of strategies. *J. Cell Biol.* **204**, 291–302.

Kelley, L. C., Hastie, E. L., Cáceres, R., Chi, Q., Schindler, A. J., Jiang, Y., Matus, D. Q., Plastino, J. and Sher (2019). Adaptive F-actin polymerization and localized

ATP production drive basement membrane invasion in the absence of MMPs. *Dev. Cell* 1–16.

Kim, H., Ishidate, T., Ghanta, K. S., Seth, M., Conte, D., Shirayama, M. and Mello, C. C. (2014). A Co-CRISPR strategy for efficient genome editing in Caenorhabditis elegans. *Genetics* **197**, 1069–1080.

Kimble, J. and Hirsh, D. (1979). The postembryonic cell lineages of the hermaphrodite and male gonads in Caenorhabditis elegans. *Dev. Biol.* **70**, 396–417.

Kohrman, A. Q. and Matus, D. Q. (2017). Divide or Conquer: Cell Cycle Regulation of Invasive Behavior. *Trends Cell Biol.* **27**, 12–25.

Lee, T., Hannett, N., Harbison, C., Thompson, C., Simon, I., Zeitlinger, J., Jennings, E., Murray, H., Gordon, D., Ren, B., et al. (2002). Transcriptional Regulatory Networks in Saccharomyces cerevisiae. *Science (80-.).* **298**, 799–804.

Levitan, D. and Greenwald, I. (1998). LIN-12 protein expression and localization during vulval development in C. elegans. *Development* **125**, 3101–3109.

Lukoseviciute, M., Gavriouchkina, D., Williams, R. M., Hochgreb-Hagele, T., Senanayake, U., Chong-Morrison, V., Thongjuea, S., Repapi, E., Mead, A. and Sauka-Spengler, T. (2018). From Pioneer to Repressor: Bimodal foxd3 Activity Dynamically Remodels Neural Crest Regulatory Landscape In Vivo. *Dev. Cell* **47**, 608-628.e6.

Maduro, M. F. (2009). Structure and evolution of the C. elegans embryonic endomesoderm network. *Biochim. Biophys. Acta - Gene Regul. Mech.* **1789**, 250–260.

Mangan, S. and Alon, U. (2003). Structure and function of the feed-forward loop

network motif. *Proc. Natl. Acad. Sci.* **100**,.

Martik, M. L. and McClay, D. R. (2015). Deployment of a retinal determination gene network drives directed cell migration in the sea urchin embryo. *Elife* **4**, 1–19.

Matus, D. Q., Li, X.-Y., Durbin, S., Agarwal, D., Chi, Q., Weiss, S. J. and Sherwood, D. R. (2010). In vivo identification of regulators of cell invasion across basement membranes. *Sci. Signal.* **3**, ra35.

Matus, D. Q., Chang, E., Makohon-Moore, S. C., Hagedorn, M. A., Chi, Q. and Sherwood, D. R. (2014). Cell division and targeted cell cycle arrest opens and stabilizes basement membrane gaps. *Nat. Commun.* **5**,.

Matus, D. Q., Lohmer, L. L., Kelley, L. C., Schindler, A. J., Kohrman, A. Q., Barkoulas, M., Zhang, W., Chi, Q. and Sherwood, D. R. (2015). Invasive Cell Fate Requires G1 Cell-Cycle Arrest and Histone Deacetylase-Mediated Changes in Gene Expression. *Dev. Cell* **35**, 162–174.

Medwig, T. N. and Matus, D. Q. (2017). Breaking down barriers: the evolution of cell invasion. *Curr. Opin. Genet. Dev.* **47**, 33–40.

Milo, R., Shen-Orr, S., Itzkovitz, S., Kashtan, N., Chklovskii, D. and Alon, U. (2002). Network motifs: simple building blocks of complex networks. *Science (80-.).* **298**, 824–827.

Morrissey, M. A., Keeley, D. P., Hagedorn, E. J., McClatchey, S. T. H., Chi, Q., Hall, D. H. and Sherwood, D. R. (2014). B-LINK: A Hemicentin, Plakin, and Integrin-Dependent Adhesion System that Links Tissues by Connecting Adjacent Basement Membranes. *Dev. Cell* **31**, 319–331.

Penn, B. H., Bergstrom, D. A., Dilworth, F. J., Bengal, E. and Tapscott, S. J. (2004).

A MyoD -generated feed-forward circuit temporally patterns gene expression dining skeletal muscle differentiation. *Genes Dev.* **18**, 2348–2353.

Porta-de-la-Riva, M., Fontrodona, L., Villanueva, A. and Cerón, J. (2012). Basic Caenorhabditis elegans Methods: Synchronization and Observation. *J. Vis. Exp.* 1–9.

Red-Horse, K., Zhou, Y., Genbacev, O., Prakobphol, A., Foulk, R., McMaster, M. and Fisher, S. J. (2004). Trophoblast differentiation during embryo implantation and formation of the maternal-fetal interface. *J. Clin. Invest.* **114**, 744–754.

Reece-Hoyes, J. S., Pons, C., Diallo, A., Mori, A., Shrestha, S., Kadreppa, S., Nelson, J., DiPrima, S., Dricot, A., Lajoie, B. R., et al. (2013). Extensive rewiring and complex evolutionary dynamics in a C.elegans multiparameter transcription factor network. *Mol. Cell* **51**, 116–127.

Rimann, I. and Hajnal, A. (2007). Regulation of anchor cell invasion and uterine cell fates by the egl-43 Evi-1 proto-oncogene in Caenorhabditis elegans. *Dev. Biol.* **308**, 187–195.

Rowe, R. G. and Weiss, S. J. (2008). Breaching the basement membrane: who, when and how? *Trends Cell Biol.* **18**, 560–574.

Sallee, M. D., Littleford, H. E. and Greenwald, I. (2017). A bHLH Code for Sexually Dimorphic Form and Function of the C. elegans Somatic Gonad. *Curr. Biol.* **27**, 1853-1860.e5.

Saunders, L. R. and McClay, D. R. (2014). Sub-circuits of a gene regulatory network control a developmental epithelial-mesenchymal transition. *Development* **141**, 1503–1513.

Schindelin, J., Arganda-Carreras, I., Frise, E., Kaynig, V., Longair, M., Pietzsch, T., Preibisch, S., Rueden, C., Saalfeld, S., Schmid, B., et al. (2012). Fiji: an open-source platform for biological-image analysis. *Nat. Methods* **9**, 676–82.

Schindler, A. J. and Sherwood, D. R. (2011). The transcription factor HLH-2/E/Daughterless regulates anchor cell invasion across basement membrane in C. elegans. *Dev. Biol.* **357**, 380–391.

Shen-Orr, S. S., Milo, R., Mangan, S. and Alon, U. (2002). Network motifs in the transcriptional regulation network of Escherichia coli. *Nat. Genet.* **31**, 64–68.

Sherwood, D. R. and Plastino, J. (2018). Invading, leading and navigating cells in caenorhabditis elegans: Insights into cell movement in vivo. *Genetics* **208**, 53–78.

Sherwood, D. R. and Sternberg, P. W. (2003). Anchor cell invasion into the vulval epithelium in C. elegans. *Dev. Cell* **5**, 21–31.

Sherwood, D. R., Butler, J. A., Kramer, J. M. and Sternberg, P. W. (2005). FOS-1 promotes basement-membrane removal during anchor-cell invasion in C. elegans. *Cell* **121**, 951–962.

Simmer, F., Tijsterman, M., Parrish, S., Koushika, S. P., Nonet, M. L., Fire, A., Ahringer, J., Plasterk, R. H. A., Louis, S., Road, T. C., et al. (2002). Loss of the Putative RNA-Directed RNA Polymerase RRF-3 Makes. *Current* **12**, 1317–1319.

Skene, P. J. and Henikoff, S. (2017). An efficient targeted nuclease strategy for high-resolution mapping of DNA binding sites. *Elife* **6**, 1–35.

Sturm, Á., Saskoi, É., Tibor, K., Weinhardt, N. and Vellai, T. (2018). Highly efficient RNAi and Cas9-based auto-cloning systems for C. elegans research. *Nucleic Acids Res.* **46**, e105.

Vega, S., Morales, A. V., Ocaña, O. H., Valdés, F., Fabregat, I. and Nieto, M. A. (2004). Snail blocks the cell cycle and confers resistance to cell death. *Genes Dev.* **18**, 1131–1143.

Verghese, E., Schocken, J., Jacob, S., Wimer, A. M., Royce, R., Nesmith, J. E., Baer, G. M., Clever, S., McCain, E., Lakowski, B., et al. (2011). The tailless ortholog nhr-67 functions in the development of the C. elegans ventral uterus. *Dev. Biol.* **356**, 516–528.

Wang, L., Shen, W., Lei, S., Matus, D., Sherwood, D. and Wang, Z. (2014). MIG-10 (Lamellipodin) stabilizes invading cell adhesion to basement membrane and is a negative transcriptional target of EGL-43 in C. elegans. *Biochem. Biophys. Res. Commun.* **452**, 328–333.

Wilkinson, H. A., Fitzgerald, K. and Greenwald, I. (1994). Reciprocal changes in expression of the receptor lin-12 and its ligand lag-2 prior to commitment in a C. elegans cell fate decision. *Cell* **79**, 1187–1198.

Xie, Q. and Cvekl, A. (2011). The orchestration of mammalian tissue morphogenesis through a series of coherent feed-forward loops. *J. Biol. Chem.* **286**, 43259–43271.

Yakoby, N., Lembong, J., Schupbach, T. and Shvartsman, S. Y. (2007). Drosophila eggshell is patterned by sequential action of feedforward and feedback loops. *Development* **135**, 343–351.

FIGURES AND FIGURE LEGENDS

Figure 1

Medwig-Kinney et al., 2019

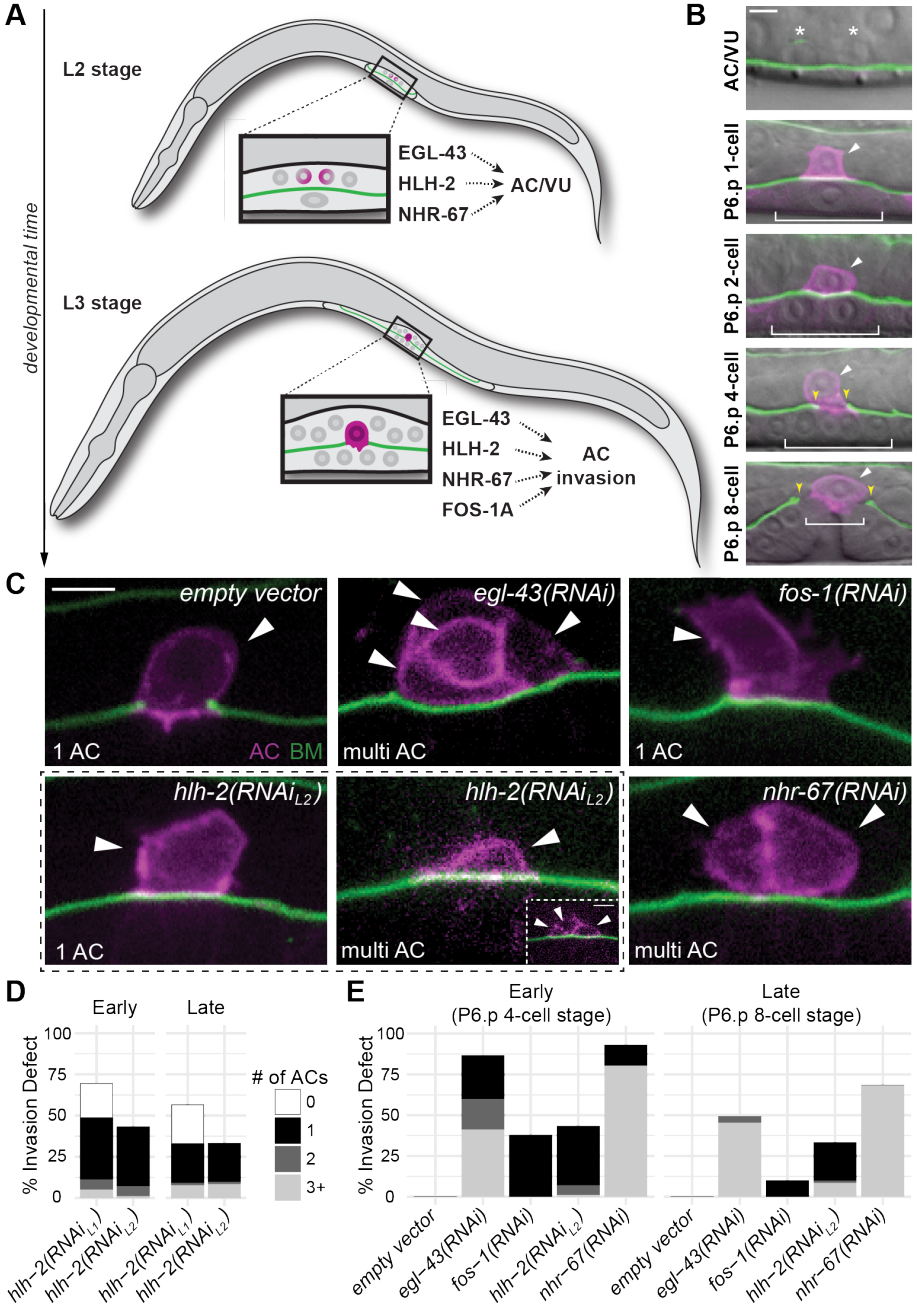

Fig. 1. RNAi depletion of pro-invasive TFs leads to defects in AC invasion and proliferation. (A) Schematic depicting the reiterative use of transcription factors in AC specification and invasion. (B) Micrographs depicting AC (magenta, *cdh-3*$^{1.5}$>mCherry::PLCδ^{PH}) specification and BM (green, *lam-1*>LAM-1::GFP) invasion over developmental time. (C) Representative empty vector control and TF-RNAi depletion phenotypes, with multiple ACs from additional confocal z-planes shown as insets. (D-E) Stacked bar charts showing the penetrance of invasion defects, binned by number of ACs, following TF-RNAi depletion (p-value < 0.00001, Fisher's exact test, empty vector compared to each TF RNAi, n ≥ 50 animals examined for each treatment). Due to the penetrance of the zero AC phenotype in early *hlh-2(RNAi)*-treated animals (D), an L2 plating strategy was used to assess post-specification AC invasion phenotypes (E).

Figure 2 Medwig-Kinney et al., 2019

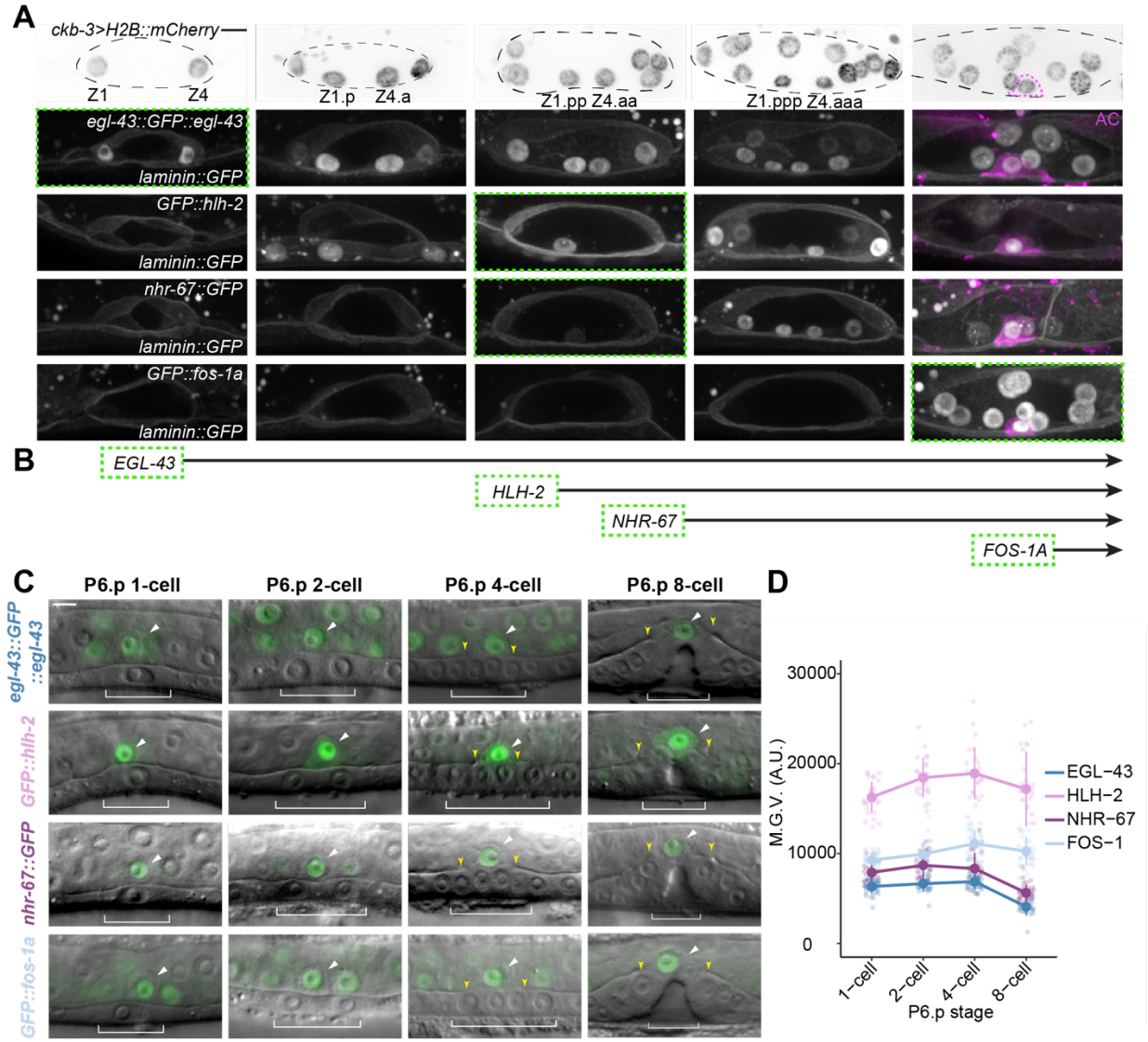

Fig. 2. Onset and expression of GFP-tagged alleles of pro-invasive TFs in the AC over developmental time. (A) Maximum intensity projections of GFP-tagged TFs (bottom) in the context of the BM-lined uterus (*laminin*::GFP), in relation to number of somatic cells in the gonad (top, *ckb-3*>H2B::mCherry, inverted). (B) Schematic illustrating the order of onset of pro-invasive TFs over time (n ≥ 25 for each stage).

Visualization (C) and quantification (D) of GFP-tagged TF levels in the AC in relation to the division of P6.p. In this and all other figures, circles and error bars denote mean ± s.d. (n ≥ 25 for each stage).

Figure 3 Medwig-Kinney et al., 2019

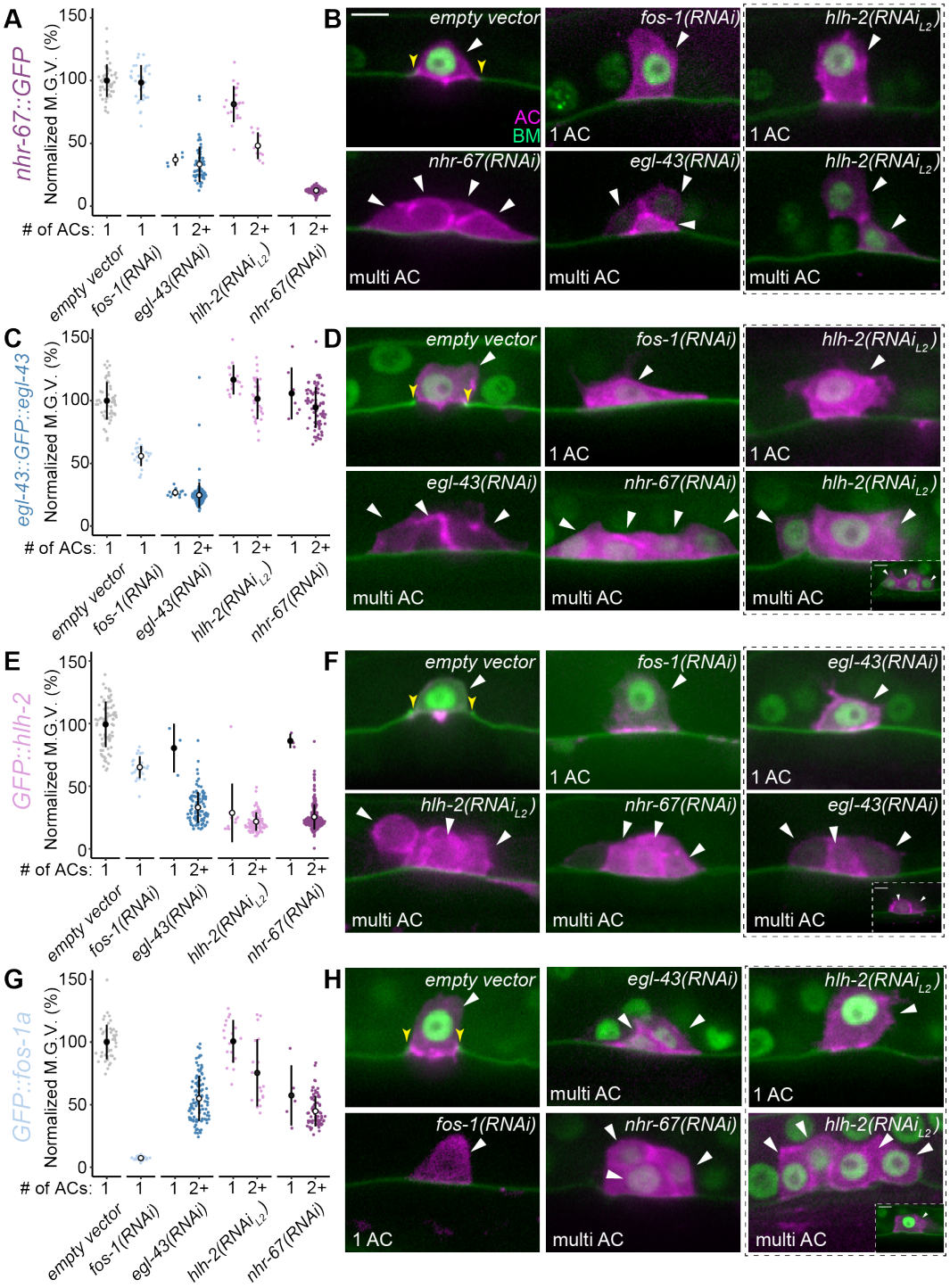

Fig. 3. Regulatory interactions among pro-invasive TFs at endogenous loci. (A, C, E, G) Sina plots of GFP-tagged TF levels, defined as the mean gray value of individual AC nuclei, following RNAi perturbation ($n \geq 25$ animals per treatment, $p < 1\times10^{-6}$, Student's t-test). (B, D, F, H) Representative phenotypes (single vs. multi AC, as noted bottom left of each image) following TF-RNAi depletion.

Figure 4 Medwig-Kinney et al., 2019

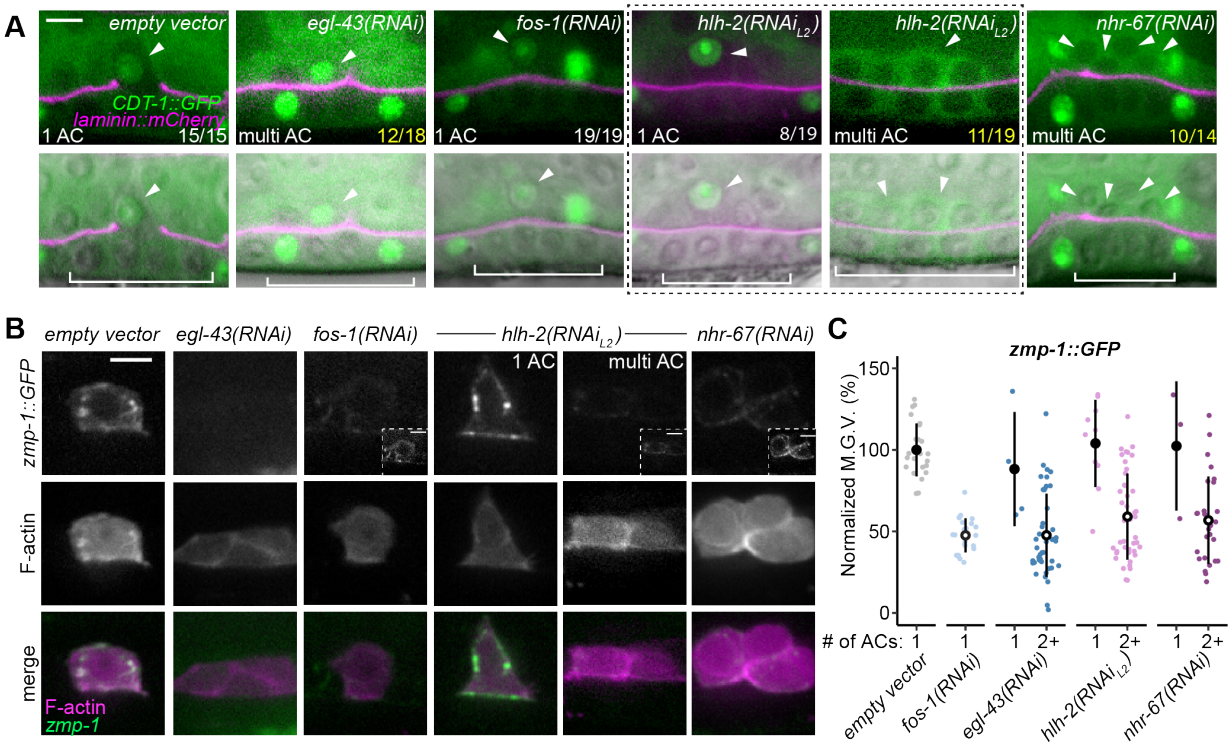

Fig. 4. Pro-invasive TFs regulate cell cycle and MMPs (A) Localization of cell cycle state reporter, *cdt-1*>CDT-1::GFP (green) and BM (*lam-1*>LAM-1::mCherry, magenta) in empty vector control (left) compared to TF-RNAi. White and yellow fractions (bottom right of each micrograph) indicate the number of animals exhibiting the phenotype shown. Visualization (B) and quantification (C) of endogenous MMP (*zmp-1::GFP*) expression in individual ACs following RNAi perturbations (n ≥ 20 animals per treatment, $p < 0.01$, Student's t-test).

Figure 5 Medwig-Kinney et al., 2019

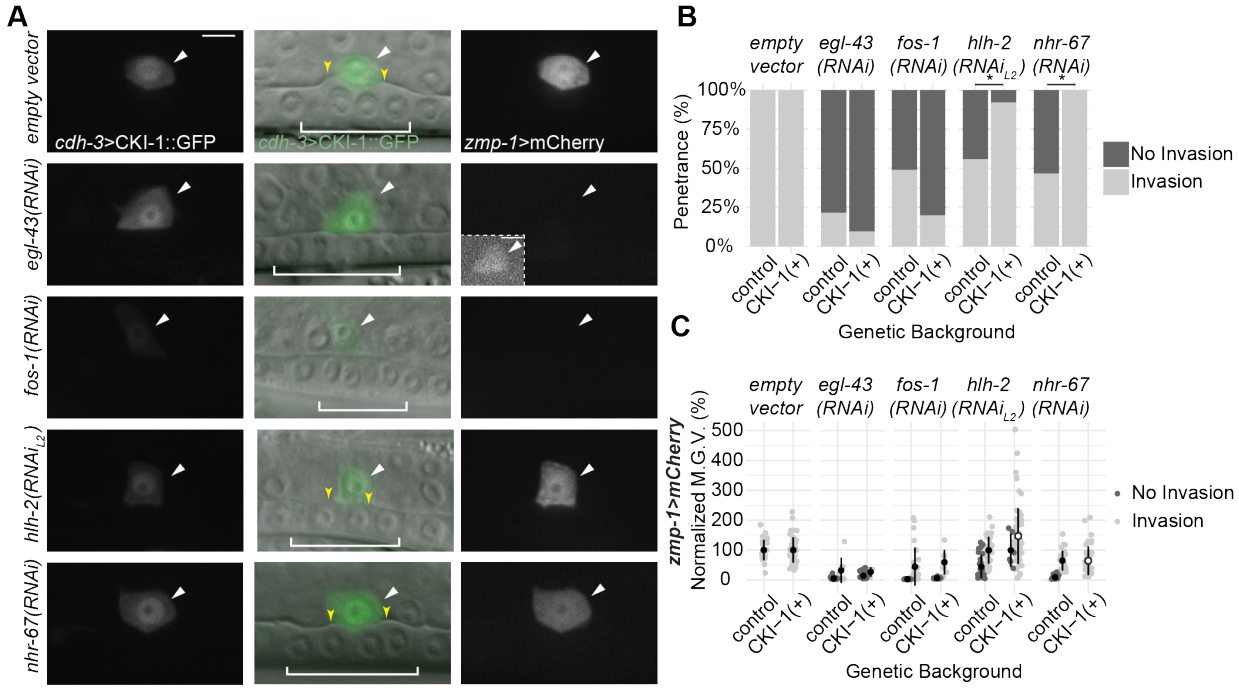

Fig. 5. HLH-2 depletion is partially rescued by induced G1/G0 arrest while EGL-43 has a cell cycle-independent pro-invasive role. (A) Micrographs depicting *cdh-3*>CKI-1::GFP (left), DIC overlay (middle), and *zmp-1*>mCherry expression (right) in empty vector control (top) and TF-RNAi depletions. (B) Quantification of AC invasion defects in control and CKI-1(+) animals (n ≥ 27 animals per treatment, p-value < 0.00001, Fisher's exact test). (C) Quantification of *zmp-1*>mCherry reporter levels in control and CKI-1(+) animals (n ≥ 27 animals per treatment, p-value of < 0.01, Student's test).

Figure 6 Medwig-Kinney et al., 2019

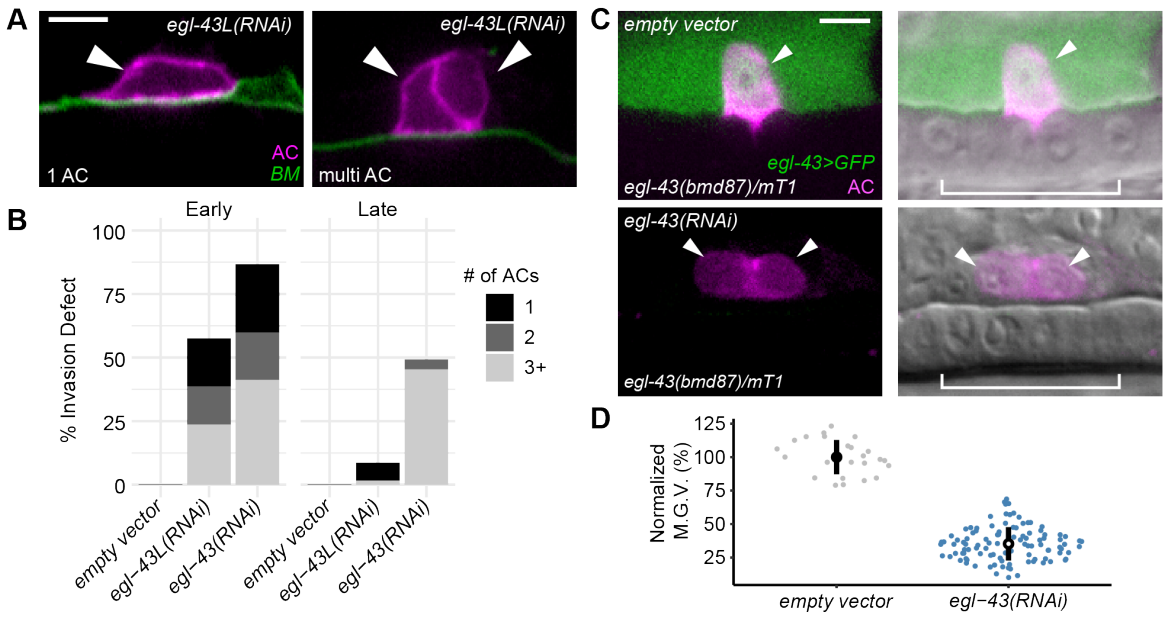

Fig. 6. Both isoforms of *egl-43* function redundantly to regulate AC invasion. Visualization (A) and quantification (B) of AC invasion and proliferation defects resulting from RNAi depletion of the long isoform of *egl-43* (*egl-43L*). Visualization (C) and quantification (D) of *egl-43*>GFP expression in individual AC nuclei, assessed using a balanced endogenous *egl-43* transcriptional reporter (*egl-43(bmd87)/mT1*), following *egl-43(RNAi)* treatment compared to control (n ≥ 25 animals per treatment, $p < 1\times10^{-15}$, Student's t-test).

Figure 7 Medwig-Kinney et al., 2019

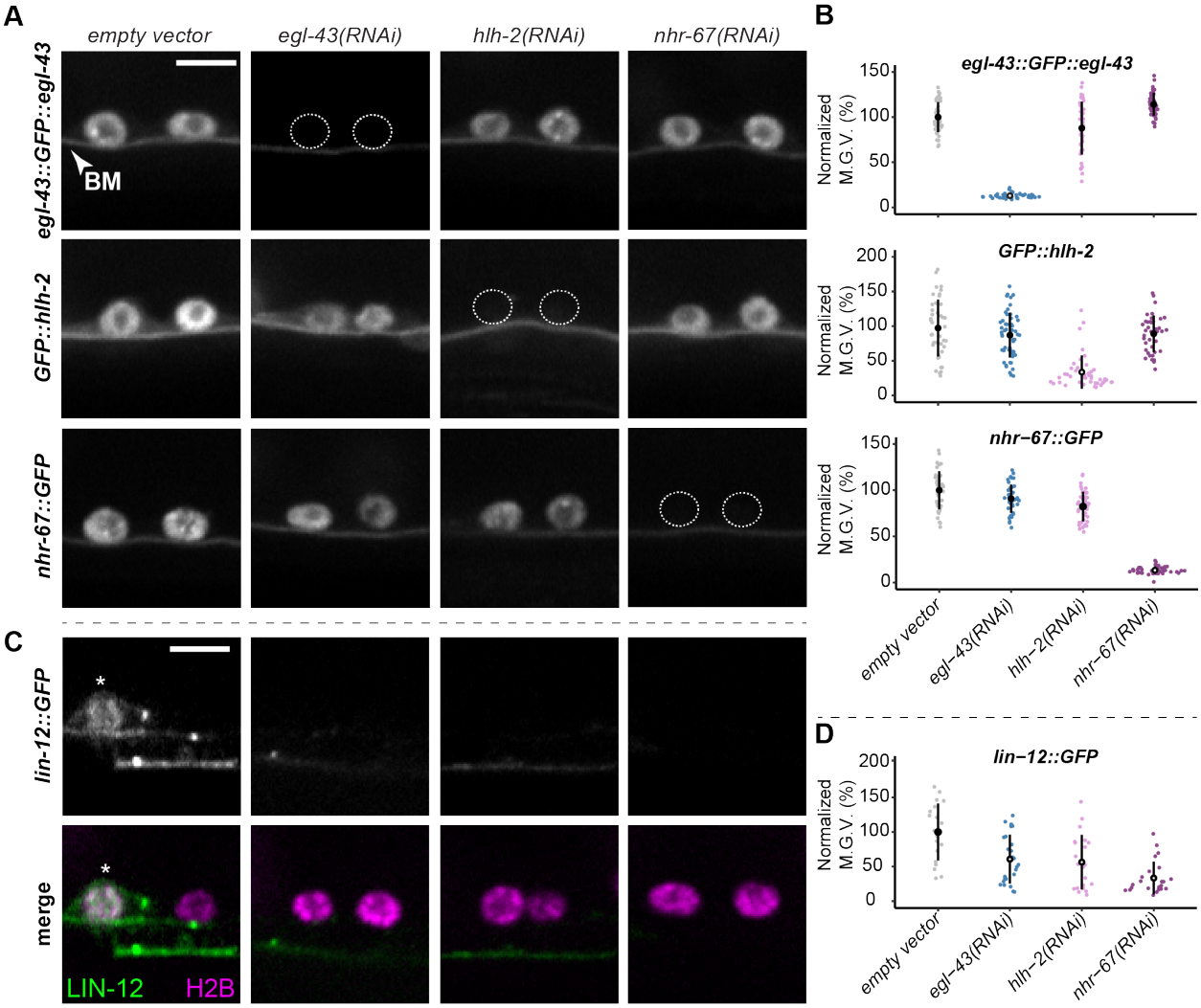

Fig. 7. Regulatory relationships do not exist prior to AC specification. Visualization (A) and quantification (B) of GFP-tagged TF levels in the AC/VU precursors (Z1.ppp and Z4.aaa) following RNAi perturbations ($n \geq 20$ animals per treatment, $p < 1 \times 10^{-6}$, Student's t-test). Visualization (C) and quantification (D) of GFP-tagged *lin-12* in the AC/VU precursors following RNAi perturbations ($n \geq 20$ animals per treatment, $p < 0.01$, Student's t-test).

Figure 8 Medwig-Kinney et al., 2019

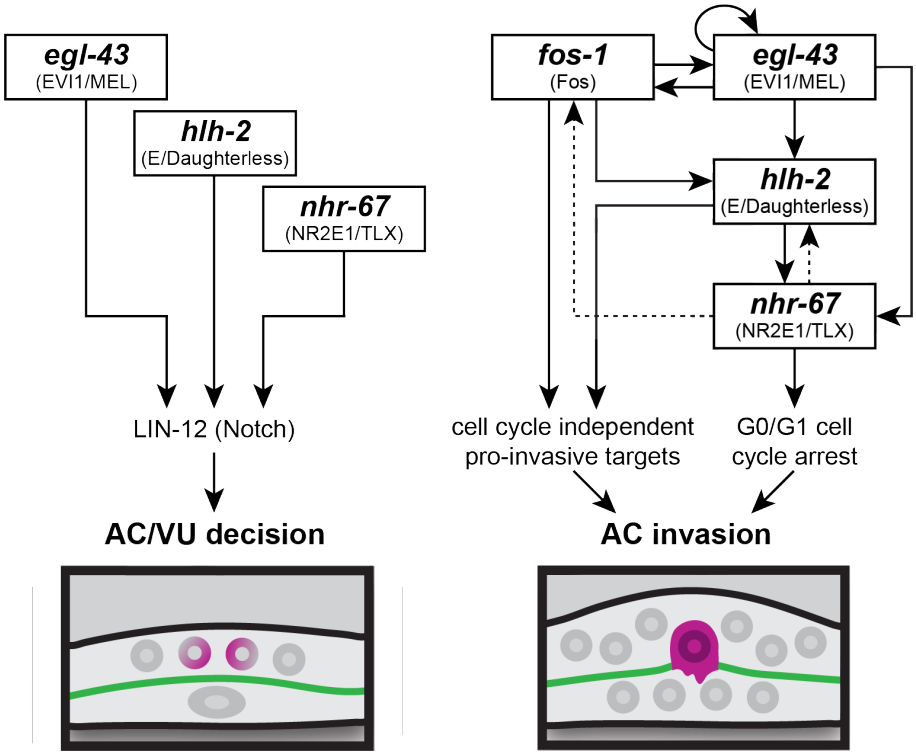

Fig. 8. Summary model of the GRNs coordinating AC specification and invasion. The Notch-mediated AC/VU cell fate decision appears to be independently regulated by *egl-43*, *hlh-2*, and *nhr-67* (left). Network inference predicts the GRN regulating AC invasion contains cell cycle independent and dependent sub-circuits, the latter entailing a type I coherent feed-forward loop with positive feedback to maintain the AC in a post-mitotic, invasive state (right). Dotted lines represent predicted feedback.